Multi-functional materials from density functional calculations

P. Ravindran, R. Vidya, and H. Fjellvåg

Center for Materials Science and Nanotechnology, Department of Chemistry, University of Oslo, P.O.Box 1033 Blindern, N-0315 Oslo, Norway.

E-mail: ravi@kjemi.uio.no

Abstract

Study on multifunctional materials is on the rise owing to their exotic fundamental properties and potential technological applications. By using accurate density-functional calculations, we attempt to understand the multifunctional properties of oxide materials and also predict new potential materials. We explore the origin of multiferroism in $BiFeO_3$, huge magneto-optical effects in double perovskites, and transparent-conducting behavior in In_2O_3.

1. Introduction

Functional materials are distinctly different with their physical and chemical properties sensitive to a change in the environment such as temperature, pressure, electric field, magnetic field, optical wavelength, etc. The functional materials utilize the native properties and functions of their own to achieve an intelligent action. Functional materials such as ferroelectric ($BaTiO_3$), magnetic-field sensor ($La_{1-x}Ca_xMnO_3$), liquid petroleum gas sensor (Pd-doped SnO_2), semiconductor light-detectors (CdS, CdTe), high-temperature piezoelectric (Ta_2O_5), fast-ion conductor, electrochromic (WO_3), and high-temperature superconductors etc. are attracting increasing attention [1]. Searching for new functional materials is a challenge for the development of smart systems. To guide this search, a clear understanding about the relationship between the physical properties and the atomic-scale structure of the materials is very much needed. In this article we describe how state-of-the-art density-functional calculations can be used to understand and predict multifunctional properties of materials very accurately. We here focus on multi-functional oxides and bring out some examples of our work on magneto-electric, magneto-optic and transparent-conducting properties.

2. Computational Details

We make use of the density-functional-theory (DFT) approach and depending upon the material and properties explored, we have chosen different computational codes. For example, to study structural stability, magneto-electric, and optical properties, we used the Vienna *ab initio* simulation package (VASP) within the projector augmented wave method [2]. For structural optimizations, the forces on the atoms were calculated using the Hellmann-Feynman theorem and they are used to perform a conjugate gradient relaxation. Structural optimizations were continued until the forces on the atoms had converged to less than 1 meV/Å and the pressure on the cell had minimized within the constraint of constant volume.

In order to calculate optical and magneto-optical (MO) spectra, we used the full-potential linear muffin-tin orbital (FPLMTO) method [3] which is an all-electron method with no shape approximation to the charge density or potential. The basis set is comprised of augmented linear muffin-tin orbitals. The spin-orbit coupling (SOC) term is included directly in the Hamiltonian matrix elements for the part inside the muffin-tin spheres, hence for spin-polarized cases the size of the secular matrix is doubled. We used a multi-basis in order to ensure a well-converged wave function and sufficiently large **k**-points in the irreducible part of first Brillouin zone: ~ 200 **k**-points for total energy studies and ~ 400 **k**-points for optical and MO studies. To describe exchange-correlation functional generalized-gradient-approximation (GGA) is used.

3. Results and Discussion

3.1. Magnetoelectric materials

Multiferroic materials have coupled electric, magnetic, and/or structural order parameters that result in simultaneous ferromagnetic, ferroelectric, and/or ferroelastic behavior. The magneto-electric materials have two order parameters, viz. spontaneous polarization for ferroelectric or antiferroelectric cases and spontaneous magnetization for ferromagnetic (F), ferrimagnetic, or antiferromagnetic (AF) cases. Coupling between the spontaneous polarization and spontaneous magnetization leads to magnetoelectric (ME) effects, in which the magnetization can be tuned by an applied electric field and vice versa. There has been considerable interest to develop multiferroic materials in which interaction between the magnetic and electronic degrees of freedom allows both charge and spin to be manipulated by applied electric or magnetic field (see Ref. 4 and references therein). These materials have opportunities for potential applications in information storage, the emerging field of spintronics, sensors, multiple-state memory elements etc. Besides the potential applications, the fundamental physics of ME materials is rich and fascinating. Hence theoretical understanding of the intrinsic physical properties of multiferroic oxides is clearly of great importance for both fundamental science and technological applications.

3.1.1. Magneto-electric studies on $BiFeO_3$

It has been believed that ferroelectricity and ferromagnetism are chemically incompatible to occur in one and the same material, because ferromagnetism arises from unequal number of majority- and minority-spin electrons localized on each atom (usually a transition-metal), whereas ferroelectricity requires d^0 electrons. However, it was shown that cation lone-pair localization also makes ferroelectric distortion e.g. in $PbTiO_3$, GeTe, Bi-compounds etc. Here we show how ferroelectric and magnetic properties exist together in $BiFeO_3$ which is a ferroelectric with Curie temperature (T_C) of 1100 K and exhibits an AF behavior with Néel temperature (T_N) of 643 K [5,6]. $BiFeO_3$ has a rhombohedrally distorted perovskite-type structure with space group $R3c$. The structural instability in perovskite-like oxides is partly related to the lattice mismatch between the cations. In order to minimize the lattice mismatch and gain stability, a lattice distortion arises by the cooperative rotation of FeO_6 octahedra along the [111] direction. Hence, three Bi-O distances are reduced, and three increased, giving rise to an octahedral distortion with rhombohedral symmetry.

By performing structural optimization in various magnetic configurations, we found that the *A*-AF-like phase is stable in energy compared to other magnetic configurations. This phase sustains ferroelectric rhombohedral distortions with large shifts of Bi atoms. The cooperative magnetism in $BiFeO_3$ originates from the half-filled and localized Fe^{3+} ($t_{2g}^3 e_g^2$) ions. The calculated magnetic moment at the Fe site in the *A*-AF-configuration is $3.724\mu_B$, in good agreement with the value of 3.752 μ_B obtained from low-temperature neutron diffraction measurements [7]. The calculated Fe magnetic moments are not integer values, since the Fe electrons have significant hybridization interaction with the neighbouring O ions. A clear insulating behaviour is observed for the *A*-AF state with band gap (E_g) of 0.97 eV.

In order to identify the "easiest" possible ferroelectric polarization path, we mapped the total energy as a function of displacement of Bi ions with respect to the FeO_6 octahedra along [001], [110], and [111] directions in the paraelectric $R\bar{3}c$ phase. The potential-energy surface associated with the displacement of Bi ion along all the three directions is having a double well shape (shown in Fig. 1). It is clear that the lowest energy off-center displacements are along the [111] direction and the polarizability of Bi

plays a special role in the ferroelectric properties

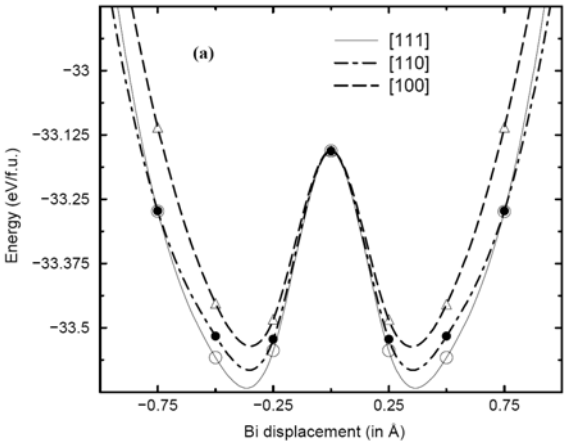

Fig. 1. Total energy as a function of displacement of Bi ion along [100], [110], and [111] directions in the *R*3*c* structure for the ferroelectric phase of $BiFeO_3$.

One of the basic quantities of ferroelectrics is spontaneous macroscopic polarization **P**, which results upon application of an electric field, and persists at zero field in two (or more) enantiomorphous metastable states of the crystal. Experiments measure **P** via hysteresis cycles from the difference Δ**P** between these metastable states. We calculated the Δ**P** between the polar (*R*3*c*) and the non-polar ($R3\bar{c}$) rhombohedral structures assuming a continuous adiabatic transformation. The calculated Δ**P** along *x*, *y*, and *z* axes in *R*3*c* structure are 1.33, 2.85, 83.53 μC/cm^2, respectively, found to be in good agreement with recent measurements [8]. Our partial polarization analysis shows that the polarization contributed by Bi, Fe, and O atoms is 86.94, 18.91, and −17.15 μC/cm^2, respectively. This indicates that the polarization contribution arising from displacement of Fe and O atoms are almost cancelling out and more than 98% of the net polarization present in $BiFeO_3$ is contributed by the Bi ions.

Electron localization function (ELF) is an informative tool to distinguish different bonding interactions in solids, so ELF for $BiFeO_3$ is shown in Fig. 2. The negligibly small value of ELF between atoms indicates the presence of dominant ionic bonding in this material. Also the ELF distribution shows the maximum value at the O sites and minimum value at the Fe and Bi sites, reiterating charge-transfer interaction from Bi/Fe to O sites. Moreover, polarization of ELF at the O sites towards the other O sites and finite ELF between Bi and O indicate the hybridization interaction. Hence it can be concluded that Bi and O as well as Fe and O have dominant ionic bonding with finite covalent character.

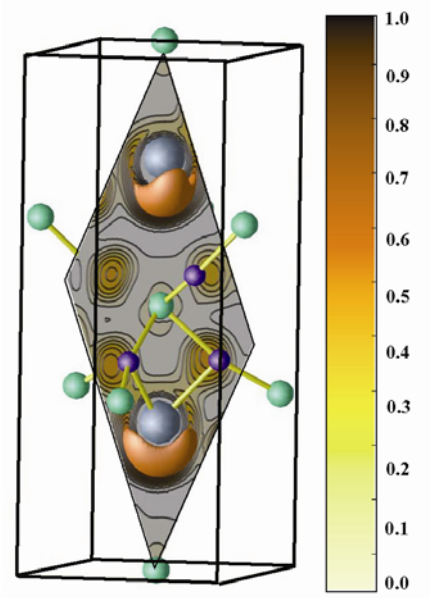

Fig. 2. Valence electron localization function (ELF) of $BiFeO_3$ in the ferroelectric *R*3*c* structure. Grey, green and violet spheres represent Bi, Fe, and O atoms, respectively. Iso-surface at a value of 0.75 enables visualization of lone pair at Bi sites.

If the bonding between the constituents of $BiFeO_3$ is purely ionic it would remain centro-symmetric (and therefore not ferroelectric), because the short-range repulsion between adjacent closed-shell ions is minimized for symmetric structures. The existence or absence of ferroelectricity is determined by a balance between these short-range repulsions (which favour the non-ferroelectric symmetric structure) and additional bonding characteristics (which stabilize the ferroelectric distortions).

By selecting an isosurface with an ELF value of 0.75, we are able to visualize

the lobe-like lone pairs around Bi (Fig. 2). It also indicates that the Bi 6*s* orbitals have direct interaction with oxygen 2*p* orbitals. In the *R*3*c* structure, half of the Bi atoms have moved in the +z direction and another half in the −z direction, breaking the symmetry and allowing hybridization between the O orbitals and the Bi p_z orbital. As a result, some of the O-p_x/O-p_y derived states are lowered in energy and move away from the Fermi surface, effectively counterbalancing the destabilization caused by the Bi lone pair. The presence of lone pair makes the hybridization interaction between Bi and O different in different directions. Moreover, the effective ionic radius of Bi ions decreases on one side and increases on the other side. Thus the Bi ions move in the [111] direction which causes a cooperative displacement of the Fe^{3+} ions due to the repulsive interaction and finally gives rise to a ferroelectric polarization. Thus $BiFeO_3$ exhibits both ferroelectric and magnetic polarizations.

3.2. Magneto-optical materials

The interaction of electromagnetic radiation with magnetized matter manifests itself as MO effects. Plane polarized light, when reflected from a metal surface or transmitted through a thin film of magnetic material will become elliptically polarized (with ellipticity ε_K in reflection mode) because, the symmetry between left-and right-hand circularly polarized light is broken due to the SOC in a magnetic solid. The MO effect due to reflection is called MO Kerr effect (MOKE) and that due to transmission is called MO Faraday effect. The major axis is rotated by an angle (θ_K in reflection mode) relative to the polarization axis of the incident beam. The polar MOKE is the most interesting and used in practical applications [9].

Materials with large MOKE have attracted a lot of attention in both basic and applied research. The motivation stems from desire to develop erasable MO memories and high density disks where digital information stored suitably in a magnetic material can be read out using MOKE. However, it is still a challenging problem to find a material with large MOKE. With the advent of modern relativistic energy-band theory [10─12] it has become possible to study the MO properties of solids quantitatively. One of the goals of theoretical MO studies is to understand the physical origins of large MO effects from aspects of the band structure, and thereby predict new suitable MO materials.

3.2.1. Magneto-optical studies on double-perovskites

Transition-metal oxides with ordered double-perovskite structure, $A_2BB'O_6$ (*A* = Ca, Sr, and Ba; *B* = Fe, and *B*' = Mo, W, and Re) are attractive as potential magnetoresistive (MR) materials [13] , half-metallic ferromagnets (HMF) or ferrimagnets with T_C in the range of 300–450 K. From full-potential DFT calculations we showed that, in addition to MR applications, these compounds can be considered for MO applications also. We found good agreement between the calculated and the available experimental MOKE spectra and hence predicted MO properties for all compounds in this series. Our work [14] was the first to point out a large MO effect in $A_2BB'O_6$ which is the largest among perovskite-like and double perovskite oxides.

As experimental MOKE is measured by applying an external magnetic field, we calculated the MO spectra in the F configuration with the easy magnetization axis along [001]. The F calculations of $Sr_2FeB'O_6$ (*B'* = Mo, W, Re) converged to be ferrimagnetic, with the magnetic moments of Fe and *B*' are antiparallel to each other. The magnetic moment of Fe is found to be around 3.57μ_B in Sr_2FeMoO_6 (SFMO), 3.99 μ_B in Sr_2FeWO_6 (SFWO), and 3.07 μ_B in Sr_2FeReO_6 (SFRO). The magnetic moment of *B*' ranges from −0.1 to −0.7 μ_B with maximum moment possessed by Re ions. The total magnetic moment is nearly an integer, i.e., 3.06 or 3.99 μ_B /f.u. Our electronic structure studies show that all these compounds have a small E_g in the majority-spin channel and a finite number of

states at the Fermi level (E_F) in the minority-spin channel and thus exhibit half-metallicity. The magnitude of E_g for SFMO, SFWO, and SFRO in the majority-spin channel is 0.59, 1.36, 0.56 eV, respectively.

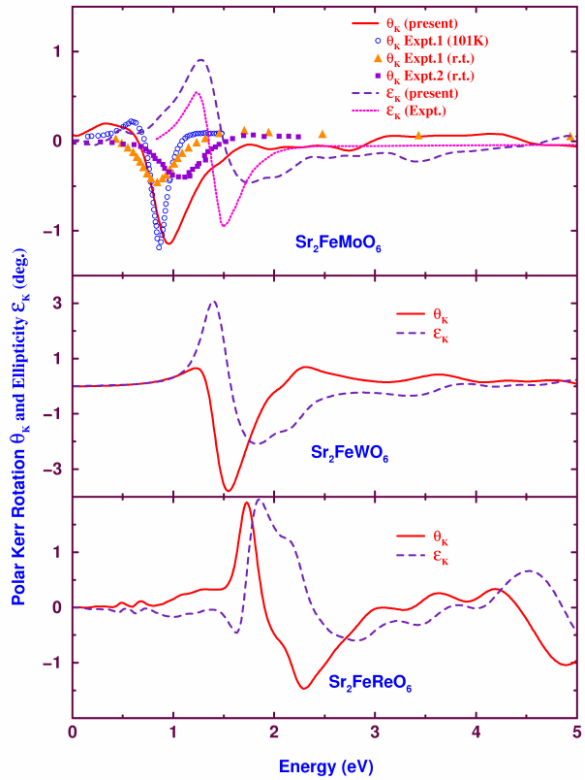

FIG. 3. Polar Kerr rotation θ_K and Kerr ellipticity ε_K spectra for $Sr_2FeB'O_6$ where B'=Mo, W, and Re. Experimental data for SFMO are taken from [Ref.15; Expt. 1] and [Ref.16; Expt. 2].

The calculated Kerr spectra for $Sr_2FeB'O_6$ together with the available experimental spectra are shown in Fig. 3. The magnitude of the calculated Kerr rotation peaks for SFMO agrees very well with that of experiment at 101 K [15]. These compounds have maximum θ_K of 1.21°, 3.87°, and 1.84° for SFMO, SFWO, and SFRO, respectively. The position of theoretical MOKE peaks are somewhat shifted in relation to the experimental ones. In general, the peaks of calculated optical conductivities and polar Kerr spectra are displaced toward higher energies with respect to experimental spectra, may be because DFT overestimates the 3*d*-band width which in turn affects the optical and MO spectra peaks. The polar Kerr ellipticity is a measure of change in the shape of the optical wave upon reflection and depends on the absolute magnitudes of the reflection coefficients. As the reflectivity of these compounds is also large, they also have large polar Kerr ellipticity.

As SFWO has the largest magnetic moment among these compounds, it exhibits larger θ_{Kmax} than SFMO and SFRO. Since the MO effect involves SOC, the MOKE is effectively correlated with spin magnetic moment. Incident photons excite the 3*d* valence electrons of the transition metals by altering their orbital angular momenta. When the electrons fall back from their excited states, the emitted photons are polarized, characteristic of both spin orientation and magnitude. The heavier the atom, the stronger will be the SO interaction. Thus, all the studied compounds have large MO effects. Moreover, SFWO has maximum exchange splitting of 3.1 eV and the largest E_g (1.36eV) in the majority spin channel. Hence the electrons are highly spin polarized in the HMF state. Therefore, larger off-diagonal conductivity, refractive index, magnetic moment, SO coupling, exchange splitting, band gap, and plasma resonance combine to give huge MO values for all the studied compounds, and in particular to SFWO. It has to be noted that a large polar Kerr rotation, typically greater than about 0.2° is clearly of benefit in reading information stored in a thermo-MO thin film. In that perspective the present compounds may be of relevance for high-density storage applications.

3.3. Transparent conducting oxides

Transparent conducting oxides (TCO) have useful features such as transparency in the visible spectrum of incident light and high electrical conductivity. The main interest for the investigation of TCO is their extensive applications such as window layers in solar cells, sensors, front electrodes in flat panel displays, low emissive windows, electro-chromic materials in rear-view mirrors of automobiles, smart windows, etc [17─ 19]. A

new field in optoelectronic device technology called transparent electronics is envisaged where TCO could lead to, for example, a functional window, which transmits visible solar radiation as well as generates electricity by the absorption of the ultraviolet portion of sunlight [20].

3.3.1. Electronic structure and optical studies on In_2O_3

One of the materials widely used as TCO is Sn-doped In_2O_3 (known as ITO) which exhibits a unique combination of optical and electrical transport properties: high optical transparency in the visible range (> 80%) and low resistivity of the order of $10^{-4}\Omega$ cm [21]. The persistent demand for better quality materials has inspired research to understand the mechanisms driving the peculiar combination of optical and electrical transport properties. It is generally accepted that the electronic band structure is one of the most important factors for understanding the unique interplay between optical absorption and electrical conductivity in these materials. Here we attempt to satisfactorily describe the interesting properties of In_2O_3 on the microscopic level by calculating the electronic band structure and optical spectra.

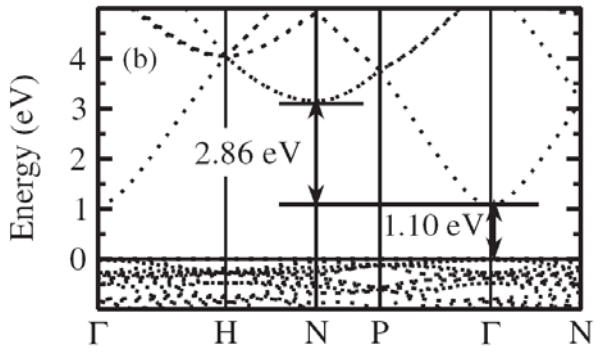

FIG. 4. Band structure In_2O_3-II, near the VB maximum and CB minimum. The Fermi level is set to zero.

The character (direct or indirect) and value of E_g are important factors for the characterization of TCO materials. We have calculated [22] the band structure for three polymorphs of In_2O_3 (shown in Fig.4 is for In_2O_3-II; $Ia\bar{3}$) within LDA and GGA. It shows that the conduction band (CB) minimum and valence band (VB) maximum are located at the Γ point. Hence, In_2O_3-II can be classified as having direct band gap. The origin for the CB minimum of In_2O_3-II is from electrons of In 5*s* orbitals with small O 2*s*, $2p_x$, $2p_y$, and $2p_z$ character. The topmost VB of In_2O_3-II contributed by electrons from O $2p_x$, $2p_y$, and $2p_z$ orbitals are slightly hybridized with the In $4d_{xy}$, $4d_{xz}$, and $4d_{yz}$ orbitals.

The remarkable feature of the calculated In_2O_3 band structure is the single free-electron-like band of *s* character forming the very bottom of the conduction band, which in turn is separated at the Γ point in the Brillouin zone by a 4 eV gap from a higher energy band having mixed O 2*p* and In 5*s* character. The high dispersion and *s*-type character of this band may also explain the high conductivity due to the high mobility of these states. The *s*-type character of these states results in a rather uniform distribution of their electronic charge density and so to their relatively low scattering.

The position, dispersion, and character of the lowest CB carry the key features responsible for electro-optic properties of TCO materials. In order to favour transparent conducting behaviour the following conditions are formulated [21]: (i) a highly dispersed and single character *s*-type band at the bottom of the CB, (ii) this band should separated from the VB by a large enough fundamental E_g to exclude inter-band transitions in the visible range, and (iii) the properties of this band are such that the plasma frequency is below the visible range. Based on the band structure analysis and the above-mentioned formulations, it can be concluded that In_2O_3 possesses *s*-electron based transparent-conducting behaviour. Effective mass characterizes band dispersion and is one of the important parameters linking electronic structure with transport properties of solids. The lowest CB of In_2O_3-II is more dispersive than the topmost VB, which means that the CB electrons are lighter than holes. Almost flat topmost VB indicates

that valence electrons are tightly bound to the atoms. Consequently, the dominant intrinsic charge carriers in In_2O_3 are expected to be electrons and not holes, consistent with experimental observations. Hence, we calculated the CB electron effective masses, and the results are (in units of the free-electron mass m_0): 0.23 (Γ-H), 0.20 (Γ-N), and 0.23 (Γ-P), whereas the experimental value is 0.30 (Γ-P).

A deeper understanding of optical properties is important from a fundamental point of view, since the optical characteristics involve not only the occupied and unoccupied parts of the electronic structure but also the character of the bands. We have calculated the imaginary parts of the optical dielectric function and derived the absorption coefficient [α(ω) in $10^5 cm^{-1}$], reflectivity [R(ω)], refractive index, and extinction coefficients etc. However here we display α(ω) and R(ω) only in Fig. 5. The optical spectra of In_2O_3-II were measured [23] for a narrow energy range 0–6 eV, which contains a peak induced by electronic transitions from the VB-maximum to CB-minimum occurring at the Γ point.

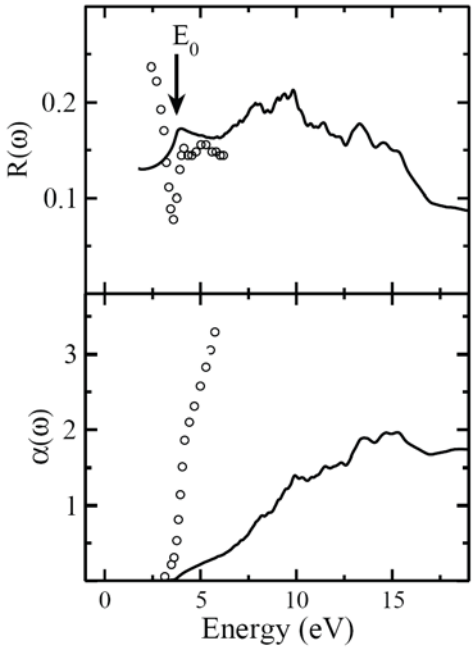

Fig.5. Calculated (solid line) reflectivity [R(ω)] and absorption coefficient [α(ω) in $10^5 cm^{-1}$] for In_2O_3-II have been compared with experimental data (circles) of Ref. 23.

The calculated reflectivity spectra agree with experimental data only at higher energies well above the E_g. The calculated absorption spectra agree with the measured spectra at lower energies. However, at energies exceeding the location of the E_0 peak, the calculated absorption coefficient is found to be much smaller than the experimentally determined values. Absorption and reflectivity spectra for this compound are low in the energy range 0–5 eV, indicating that it will be optically transparent.

4. Conclusions

In brief, we conclude that our calculations show that the easy axis of ferroelectric polarization is along the [111] direction in $BiFeO_3$, consistent with experimental observation. The ferroelectricity in $BiFeO_3$ is originating from the distortion of Bi-O coordination environment as a result of the stereochemical activity of the lone pair on Bi. Large anisotropy in the polarization of $BiFeO_3$ has been identified and this could explain why there is large scattering in the experimentally reported polarization values in this material. This demonstrates that accurate DFT calculations can be used to explore not only the structural and magnetic properties but also the ferroelectric properties of magnetoelectric materials.

The $Sr_2FeB'O_6$ compounds (B' = Mo, W, and Re) exhibit huge magneto-optical effects, owing to the large perpendicular magnetic anisotropy due to non-cubic structure, large magnetic moment on Fe, large spin-orbit coupling from B', and larger off-diagonal conductivity etc. Sr_2FeWO_6 (SFWO) is found to have the maximum polar Kerr rotation (3.87°). As these compounds have large Kerr rotation (more than 1°), they are promising for technological applications.

The absorption and reflectivity of In_2O_3 are low in 0–5 eV, leading to its optically-transparent behaviour. A well-dispersive s-like band at the conduction band

minimum and more-localized bands at the valence-band minimum lead to conductivity in this material. As effective mass of electrons in the conduction band is less than that of holes, In_2O_3 has n-type conductivity. The present work clearly elucidates that density-functional theory is able to explain almost all properties of multifunctional materials. Hence it is a reliable tool to predict new interesting materials useful in multifunctional devices.

Acknowledgement

The authors are grateful to the Research Council of Norway for financial support and computer time in Norwegian supercomputer facilities.

References:

1. H. Donnerberg, *Atomic simulation of electro-optic and magneto-optic oxide materials* Springer-Verlag, Berlin (1999).
2. G. Kresse and J. Furthmüller, Phys. Rev. B **54**, 11169 (1996).
3. J.M. Wills, O. Eriksson, M. Alouani, and D.L. Price, in *Electronic Structure and Physical Properties of Materials*, edited by H. Dreysse (Springer, Berlin, 2000), p. 148.
4. P. Ravindran, R. Vidya, A. Kjekshus, H. Fjellvåg, and O. Eriksson, Phys. Rev. B **74**, 224412 (2006).
5. V. G. Bhide and M. S. Multani, Solid State Commun. **3**, 271 (1965).
6. Y. N. Venevtsev and V. V. Gagulin, Inorg. Mater. **31**, 797 (1995).
7. I. Sosnowska, W. Schäfer, W. Kockelmann, K. H. Andersen, and I. O. Troyanchuk, Appl. Phys. A: Mater. Sci. Process. **74**, S1040 (2002).
8. J. Wang, J. B. Neaton, H. Zheng, V. Nagarajan, S. B. Ogale, B. Liu, D. Viehland, V. Vaithyanathan, D. G. Schlom, U. V. Waghmare, N. A. Spaldin, K. M. Rabe, M. Wutting, and R. Ramesh, Science **299**, 1719 (2003).
9. P. Ravindran, A. Delin, P. James, B. Johansson, J.M. Wills, R. Ahuja, and O. Eriksson, Phys. Rev. B **59**, 15680 (1999).
10. P.M. Oppeneer, J. Sticht, F. Herman, J. Magn. Soc. Jpn. **15** (S1), 73 (1991).
11. S.V. Halilov, R. Feder, Solid State Commun. **88** (1993) 749.
12. G.Y. Guo, H. Ebert, Phys. Rev. B **50,** 10377(1994).
13. K.-I. Kobayashi, T. Kimura, H. Sawada, K. Terakura, and Y. Tokura, Nature **395**, 677 (1998).
14. R. Vidya, P. Ravindran, A. Kjekshus, and H. Fjellvåg, Phys. Rev. B **70**, 184414 (2004).
15. K. Shono, M. Abe, M. Gomi, and S. Nomura, Jpn. J. Appl. Phys. Part 1 **21**, 1720 (1982).
16. T. Kise, T. Ogasawara, M. Ashida, Y. Tomioka, Y. Tokura, and M. Kuwata-Gonokami, Phys. Rev. Lett. **85**, 1986 (2000).
17. H. Kawazoe, M. Yasukawa, H. Hyodo, M. Kurita, H. Yanagi, and H. Hosono, Nature **389**, 939 (1997).
18. Thomas, Nature **389**, 907 (1997).
19. F. Wager, Science **300**, 1245 (2003).
20. H. Sato, T. Minami, S. Takata, and T. Yamada, Thin Solid Films **236**, 27 (1993).
21. O. N. Mryasov and A. J. Freeman, Phys. Rev. B **64**, 233111 (2001).
22. S. Zh. Karazhanov, P. Ravindran, P. Vajeeston, A. Ulyashin, T. G. Finstad, and H. Fjellvåg, Phys. Rev. B **76**, 075129 (2007).
23. I. Hamberg, C.G. Granqvist, K.F. Berggren, B.E. Sernelius, and L. Engström, Phys. Rev. B **30**, 3240 (1984).